Available online at www.sciencedirect.com
ScienceDirect
Ceramics International 37 (2011) 1333–1339
CERAMICS INTERNATIONAL
www.elsevier.com/locate/ceramint

Studies on plasma sprayed bi-layered ceramic coating on bio-medical Ti–13Nb–13Zr alloy

S. Sathish [a], M. Geetha [a], S.T. Aruna [b,*], N. Balaji [b], K.S. Rajam [b], R. Asokamani [a]

[a] School of Mechanical and Building Sciences, VIT University, Vellore 632014, India
[b] Surface Engineering Division, Council of Scientific and Industrial Research-National Aerospace Laboratories, Bangalore 560017, India

Received 7 September 2010; received in revised form 15 November 2010; accepted 13 December 2010
Available online 21 January 2011

Abstract

Biomedical Ti alloys are prone to undergo degradation due to the combined effect of wear and corrosion. To overcome these problems, surface modification techniques are being used. In this paper, the biomedical Ti alloy Ti–13Nb–13Zr was plasma sprayed with nanostructured Al_2O_3–13 wt%TiO_2, yttria stabilized zirconia powders and bilayer containing alternate layers of the two coatings to improve the corrosion resistance and microhardness of the substrate. The plasma sprayed coatings were characterized by X-ray diffraction, scanning electron microscopy and Raman spectroscopy. The microstructure, microhardness and surface roughness of the coatings were investigated. The corrosion resistance of the coatings was studied in simulated body conditions. The results show improved corrosion resistance for the bilayered coating compared to the individual plasma sprayed coatings on biomedical Ti–13Nb–13Zr alloy substrate.

Keywords: B. X-ray methods; C. Corrosion; C. Hardness; D. ZrO_2; E. Biomedical applications

1. Introduction

With an ageing population, increasing accidents and sports related injuries there is an ever-increasing demand for hard tissue replacement such as bone. Titanium and its alloys are being extensively used for orthopedic implants such as hip and knee replacements because of their high strength to weight ratio, superior corrosion resistance and biocompatibility [1]. However, they are prone to undergo degradation after 10–15 years due to the combined effect of wear and corrosion [2]. In order to overcome this problem, surface modification techniques such as ion implantation, laser surface modification, plasma spraying, etc., are being used for protecting the implants against wear and corrosion [3–5]. Amongst the above, plasma spraying is preferred due to its simplicity, robustness and cost effectiveness compared to other techniques. The recent trend in plasma spraying is to use reconstituted nanostructured powders to obtain a coating with bimodal microstructure, which can improve the properties of the coating. It has been reported that the properties like adhesion strength, abrasive wear resistance and spallation resistance of the nanostructured Al_2O_3–13 wt%TiO_2 (AT) coatings were remarkably increased when plasma sprayed on mild carbon steel substrate [6,7]. Nanostructured AT coatings have been employed in naval ships and submarines due to its better wear and corrosion resistance [8]. Further, it has been demonstrated that the nanostructured ceramic materials exhibit enhanced biocompatibility when compared to the conventional powders [9]. Implants made of alumina (Al_2O_3), zirconia (YSZ) and coatings of titania (TiO_2) are known to be biocompatible [10–12]. A recent paper by Ma et al. reports enhanced thermal cyclic life time of bilayered ($La_2Ce_2O_7$/8YSZ) coatings on nickel based super alloy compared with the single layered ($La_2Ce_2O_7$) coating for TBC application [13]. Apart from this, to the best of our knowledge there is no report on plasma sprayed AT as well as coatings with bilayers of YSZ and AT on biomedical implant alloys for improving their corrosion resistance. In this regard, the present work is the first of its kind wherein the effect of plasma sprayed AT, YSZ and alternate layers of YSZ and AT coatings on corrosion resistance of biomedical titanium alloy (Ti–13Nb–13Zr) has been investigated.

* Corresponding author. Tel.: +91 080 25086250; fax: +91 080 25210113.
E-mail address: aruna_reddy@nal.res.in (S.T. Aruna).

0272-8842/$36.00
doi:10.1016/j.ceramint.2010.12.012

2. Experimental

2.1. Characterization of plasma sprayable powders

Reconstituted nanostructured Al_2O_3–13 wt%TiO_2 (AT) and 7 wt% yttria stabilized zirconia (YSZ) powders procured from Inframat Corporation were used. Phase analysis of the starting powders were performed on Philips 3121 X-ray diffractometer using Cu Kα radiation which was set at 40 kV and 20 mA for the XRD analysis and the data were recorded in the 2θ range 10–80° in steps of 2°/min. The surface morphologies of the starting powders were observed by JEOL JSM-6360 scanning electron microscope (SEM).

2.2. Plasma spraying and characterization of the plasma sprayed coatings

Ti–13Nb–13Zr alloy substrate (35 mm × 20 mm × 4 mm) was grit blasted using cabinet type grit blasting machine (Sandstorm equipment, India) using alumina grits (20 μm) prior to plasma spraying. The substrate was positioned at a distance of 15 mm from the grit blasting gun and the angle between the grit blasting gun and the substrate was maintained at 90°. Plasma spraying of the reconstituted nanostructured powders was carried out using 80 kW plasma spray system (Sulzer Metco 9MB). The samples were preheated to a temperature of 400 °C by means of the plasma torch before plasma spraying so as to enhance the adhesion of the coating. Three different coatings, viz., AT, YSZ and AT over YSZ were plasma sprayed on to the substrate and the coatings are schematically represented in Fig. 1. The plasma spray parameters used for AT and YSZ coatings on Ti–13Nb–13Zr alloy are listed in Table 1. It is important to mention that the same processing parameters given in Table 1 were used to deposit the bilayered coating. The carrier gas flow rate was kept constant for all the coatings.

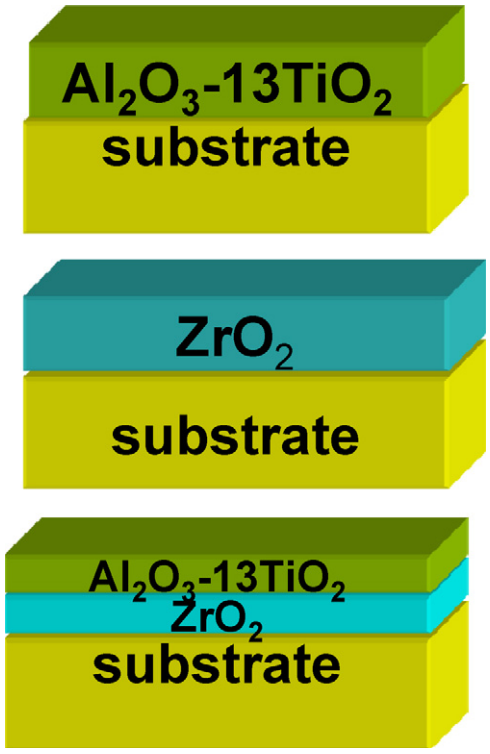

Fig. 1. Schematic diagrams of (a) AT coating, (b) YSZ coating and (c) bilayer coating.

Table 1
Plasma spray parameters used for plasma spraying AT and YSZ powders.

Parameters	YSZ coating	AT coating
Plasma current (A)	450	600
Plasma voltage (V)	55	50
Ar gas flow pressure (NLPM)	42	42
H_2 gas flow pressure (NLPM)	8	9
Carrier gas flow (psi)	58	58
Spray distance (cm)	20	20

The phases present in the plasma sprayed coatings were identified by XRD. The phase analysis of the coatings was also carried out using Raman spectrometer (DILOR-JOBIN-YVON-SPEX). The surface morphologies and the cross-sectional images of the coatings were observed by SEM. For cross-sectional SEM studies, the samples were mounted using bakelite powder followed by grinding and polishing with emery papers of different grit sizes, ranging from 120 μm to 1600 μm and mirror finished by 1 μm diamond paste. Microhardness measurements were carried out on the cross-section of the coated samples using micro Vickers hardness tester (Chennai Metco). A load of 200 g was applied for 15 s and the microhardness values were measured on ten different places on the cross-section and its standard deviation is reported. The thickness of the plasma sprayed AT, YSZ and BL-1 (∼100 μm YSZ + ∼100 μm AT) coatings were ∼200 μm. A bilayered coating with 200 μm each of YSZ and AT was also plasma sprayed (BL-2). The average surface roughness of the coatings was measured using Talysurf FTS 50 profilometer (Taylor Hobson Make). Porosity measurements were carried out on the microstructures of the SEM images using MATERIAL-PRO Software attached with optical microscope.

2.3. Electrochemical corrosion behaviour of coatings

Potentiodynamic polarization experiments were carried out on the bare substrate Ti–13Nb–13Zr alloy (1 cm × 1 cm) as well as the plasma sprayed coatings in simulated body fluid (Hank's solution: 0.185 g/l $CaCl_2$, 0.4 g/l KCl, 0.06 g/l KH_2PO_4, 0.1 g/l $MgCl_2{\cdot}6H_2O$, 0.1 g/l $MgSO_4{\cdot}7H_2O$, 8.0 g/l NaCl 0.35 g/l $NaHCO_3$, 0.48 g/l Na_2HPO_4 and 1.00 g/l D-glucose) to evaluate their corrosion resistance. All the potential measurements were made with reference to a saturated calomel electrode (SCE) as reported [14]. A platinum foil was used as counter electrode and an electrochemical interface (Gill AC, ACM make) was used for conducting the experiments. For the electrochemical measurements, the substrates with and without the plasma sprayed coatings were placed in a Teflon holder, with a 6 mm diameter window and exposed to the solution. Open circuit potential (OCP)-time measurements were carried out for an hour to achieve a steady open-circuit potential, which

was measured as the corrosion potential. When the specimen attained a constant potential, potentiodynamic polarization was started from an initial potential of 250 mV below the OCP. The scan rate used was 0.166 mV s^{-1} as per ASTM F2129 standards. The experiments were repeated thrice to check the repeatability. Electrochemical impedance spectroscopy (EIS) measurements were performed with the same experimental setup used for potentiodynamic polarization studies. The frequency response analyzer and potentiostat were driven by Z plot software. Impedance measurements were carried out with a frequency sweep ranging from 10,000 Hz to 1 Hz. The software led to obtain the best fit from the acquired data, which in turn led to smooth and reliable curves.

3. Results and discussion

3.1. Phase analysis by XRD and Raman spectroscopy

Fig. 2 shows the XRD patterns of the nanostructured YSZ powder and plasma sprayed YSZ coating. The XRD patterns of both the YSZ powder and the coating were found to be similar. All the peaks corresponding to tetragonal zirconia phase were observed and peaks corresponding to cubic zirconia were not distinct. The crystallite sizes of the YSZ powder as calculated from Scherrer formula were 26 nm for tetragonal zirconia. The Raman spectra of plasma sprayed YSZ coating showed peaks at 149 cm^{-1} (B_{1g}), 191 cm^{-1}, 322 cm^{-1} (B_{1g}), 466 cm^{-1} (E_g) and 639 cm^{-1} (E_g) corresponding to tetragonal zirconia and a peak around 247 cm^{-1} which corresponds to cubic zirconia [15]. Thus Raman spectroscopy results show the presence of cubic zirconia phase which was not evident from XRD.

The XRD patterns of AT powders and plasma sprayed AT, and BL coatings are shown in Fig. 3. The XRD pattern of AT powder showed diffraction peaks corresponding to α-Al_2O_3, γ-Al_2O_3, δ-Al_2O_3, brookite, anatase and rutile TiO_2 (Fig. 3a). Additional peaks corresponding to CeO_2 and ZrO_2 were also seen and similar observation has been reported by Sanchez et al. [16]. Such additives are incorporated into the powder so as to reduce the sintering temperature and enhance the densification process. The average crystallite size calculated from Scherrer formula for AT powder were 52 nm and 64 nm, respectively, for α-Al_2O_3 and rutile TiO_2 phases.

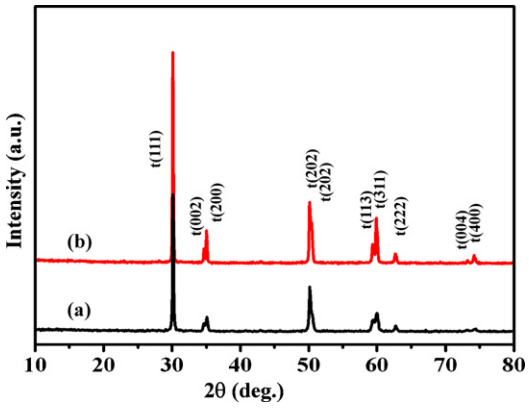

Fig. 2. XRD patterns of (a) YSZ powder and (b) YSZ coating.

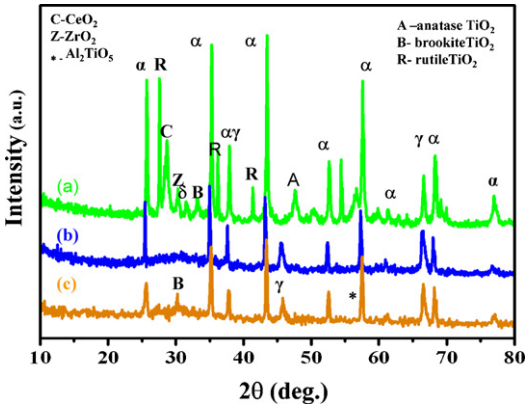

Fig. 3. XRD patterns of (a) AT powder, (b) AT coating and (c) bilayer coating.

The XRD pattern of plasma coated AT surface (Fig. 3b) showed a mixture of α-Al_2O_3 and γ-Al_2O_3 along with Al_2TiO_5. The peaks observed around 25–35° in the XRD pattern of AT powder were not observed in the XRD pattern of plasma sprayed AT coating and instead a broad hump was noticed. The broadened XRD peak in the coating indicates nucleation of amorphous phases. The presence of γ-phase in the coated surface is due to the complete melting of the starting powder and also due to the fact that γ-Al_2O_3 commonly nucleates in preference to α-Al_2O_3 during rapid solidification of liquid droplets [17–19]. Peaks corresponding to Al_2TiO_5 phase were also observed in the XRD pattern of the AT coating which could have resulted from the reaction between Al_2O_3 and TiO_2 in the plasma flame. Peaks corresponding to rutile titania were not observed in the XRD pattern of plasma sprayed AT surface. This may be due to the negligible solubility of TiO_2 in the equilibrium α-Al_2O_3. As a result, Ti ions are likely to be in the γ-Al_2O_3 lattice as either an interstitial or substitutional defect [6]. Similar observations have been reported by several researchers [20,21]. However, the Raman spectra showed peaks at 263, 438 and 604 cm^{-1} corresponding to rutile TiO_2. The crystallite size of the AT coating calculated from Scherrer formula was approximately 55 nm for α-Al_2O_3 and 31 nm for γ-Al_2O_3. This clearly indicates that there is not much of a grain growth during plasma spraying of AT powder.

The XRD pattern of the BL coating is shown in Fig. 3c. It shows the presence of α-Al_2O_3, γ-Al_2O_3, Al_2TiO_5 and brookite TiO_2. Some authors have also observed the brookite phase formation and no explanation has been given [21,22]. It is interesting to note that brookite TiO_2 was absent in the plasma sprayed AT monolayer coating. Brookite being a metastable phase could have resulted from rapid quenching of the splats. The crystallite sizes were 11 nm, 13 nm, 47 nm and 2 nm, respectively, for α-Al_2O_3, γ-Al_2O_3, Al_2TiO_5 and brookite TiO_2. Peaks corresponding to YSZ were not seen in the XRD pattern. This is due to the fact that the YSZ coating was below the AT coating. On the other hand, Raman spectra of BL coating showed a peak at 639 cm^{-1} corresponding to tetragonal zirconia. Two peaks were also observed at 871 cm^{-1} and 986 cm^{-1} which can be assigned to the mineral phase of corundum–ruby as reported in literature [23].

3.2. Microhardness and microstructure of plasma sprayed coatings

The Vickers microhardness of all the coatings was found to be higher when compared to that of the uncoated Ti–13Nb–13Zr alloy. The BL coating possesses substantially a higher microhardness value (1096 ± 10 HV) which is ∼1.3 times that of AT (820 ± 22 HV) and ∼1.8 times that of YSZ coatings (617 ± 25 HV). The increase in the microhardness of the BL coating may be attributed to the presence of more of fully melted splats in the microstructure of the coating.

The SEM images of plasma sprayed AT coatings surface and EDAX spectra are shown in Fig. 4. The microstructure of AT coating consisted of both fully melted and partially melted regions (Fig. 4a) which are typical of a bimodal microstructure [24]. The unmelted region consisted of smaller size particles mostly in the nanosize range (Fig. 4b). EDAX spectra of unmelted region mainly composed of alumina particles (Fig. 4c). The EDAX spectral data is tabulated in Table 2. High resolution SEM image of the partially melted region is shown Fig. 5. Two kinds of microstructure can be seen in partially melted regions, liquid phase sintered region and a solid phase sintered region. The existence of the liquid phase sintered region is due to the selective melting of TiO_2 nanoparticles during plasma spraying whereas the solid phase sintered regions are composed of nanoparticles of Al_2O_3–TiO_2 in unmelted state during plasma spraying [21].

The formation of bimodal microstructure can be attributed to the fact that the heat transfer within the agglomerated particles is lower compared to the dense feed stock. Upon impact, the outer shell of the agglomerated nanoparticles solidifies to form micron sized zones while the inner core will retain its nanosized structure [24]. Apart from the above mentioned primary reason, the other contributing factor may be due to the differences in the melting point of alumina (2015 °C) and titania (1640 °C). Thus titania can melt completely in the plasma flame and unmelted alumina particles can get embedded in the melted titania. The porosity of AT coating as calculated from the SEM image is found to be 0.6%.

Table 2
EDAX data recorded on the surface of plasma sprayed AT coating.

Point on the SEM image	Element wt% (±%error)		
	Oxygen	Aluminium	Titanium
1	39.50 (0.61)	51.63 (0.25)	8.87 (0.26)
2	37.33 (0.40)	51.89 (0.26)	10.78 (0.29)
3	36.85 (0.39)	51.85 (0.26)	11.29 (0.30)
4	42.09 (0.46)	45.14 (0.25)	12.77 (0.36)

The SEM images showing the surface morphology of YSZ coatings and cross-section of BL coating are shown in Fig. 6. The surface morphology of the YSZ coated surface is composed of more number of fully melted zones, poorly consolidated fine particles with large number of pores (3.5%) and cracks (Fig. 6a). The presence of poorly consolidated particles in the coating can be attributed to the lower heating rate in the plasma torch and higher momentum of the starting powders [17]. The reason for the difference in the melting behaviours of both the YSZ and AT coatings can also be due to the fact that the specific heat capacity (450 J/kg) and latent heat

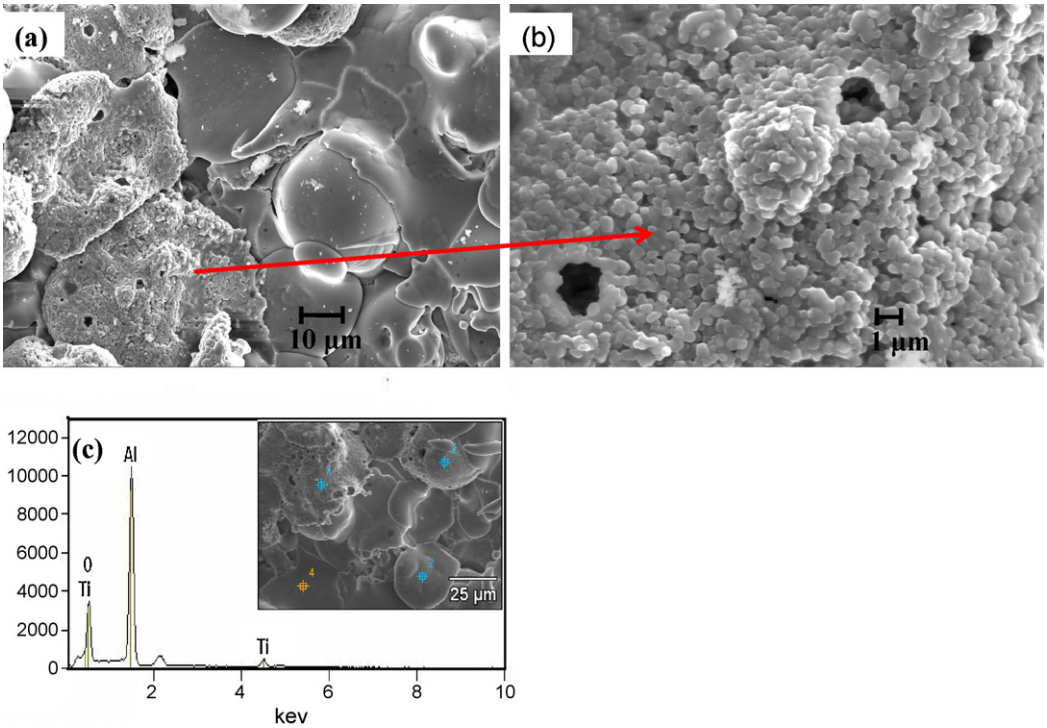

Fig. 4. SEM images of surface of plasma sprayed AT coating: (a) bimodal nature, (b) unmelted region showing nanosize particles and (c) a typical EDAX spectra of plasma sprayed AT coating.

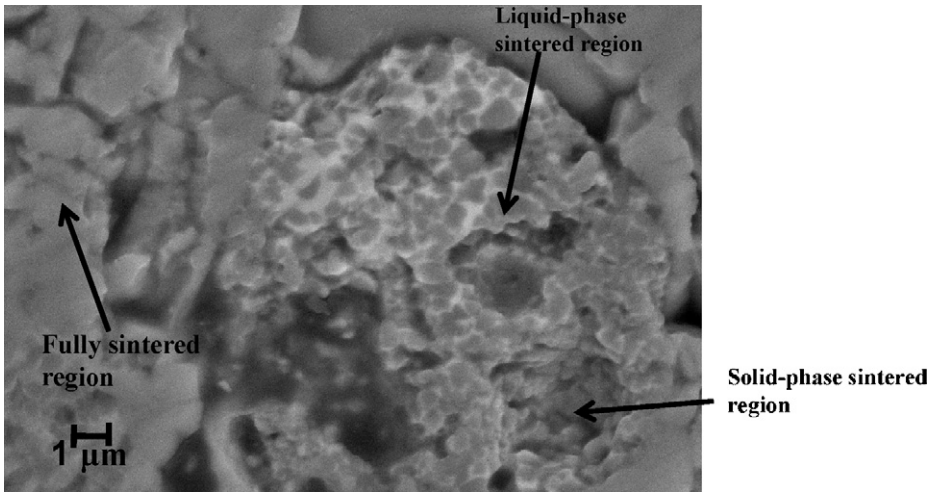

Fig. 5. High magnification SEM image of partially melted region of AT coating.

(750 J/(kg K)) of YSZ are much lower than the specific heat capacity (750 J/(kg K)) and latent heat (1500 J/(kg K)) of AT. In addition, the YSZ has higher specific mass (6000 kg/m^3) than AT (4000 kg/m^3) leading to higher void content in YSZ when compared to AT coating. The surface morphology of the BL coating showed the presence of a large number of fully melted splats, with very less porosity (0.01%). There was a complete melting of alumina particles in the BL coating which may be due to the lower thermal conductivity of the bottom YSZ layer (thermal conductivity of zirconia, alumina and titania are 2–2.5 W m^{-1} K, 18 W m^{-1} K and 8.8 W m^{-1} K, respectively). The AT coating in the bilayered coating had good adhesion with the already deposited YSZ layer (Fig. 6). The discrepancies in the microstructures of the BL and YSZ Coatings may be due to the fact that in BL Coating, the initially deposited zirconia layer is already heated by the plasma flame to a higher temperature compared to the bare substrate. It is reported in the literature that higher substrate temperature will result in the formation of well layered lamellae which in turn results in higher microhardness and reduced porosity of the plasma sprayed coatings [25]. It is important to mention that the bond coat (NiCrAlY) that is widely used for coating AT was not considered in our studies as Ni is not biocompatible [26] and we propose YSZ to act as the bond coat for biomedical Ti alloys.

The average surface roughness of plasma sprayed coatings was in the range of 6–10 µm. The bilayer coating exhibited the lowest surface roughness of 6 µm.

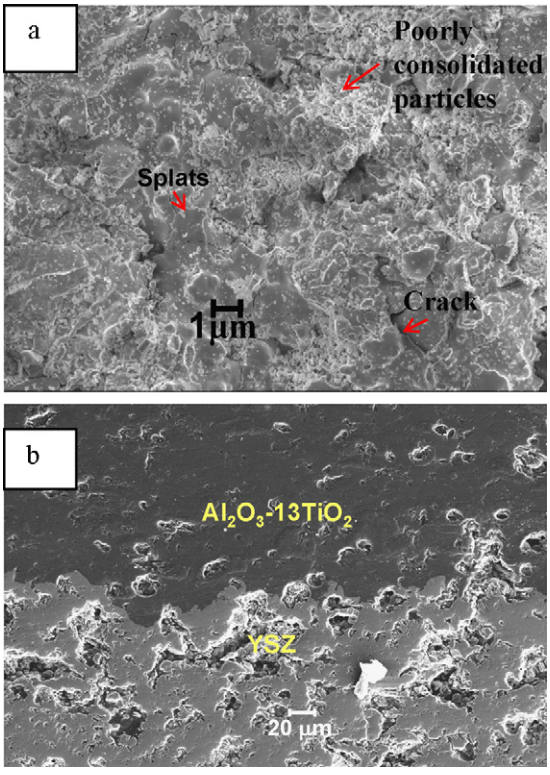

Fig. 6. (a) SEM image of the surface of plasma sprayed YSZ coating and (b) cross-sectional SEM image of BL coating.

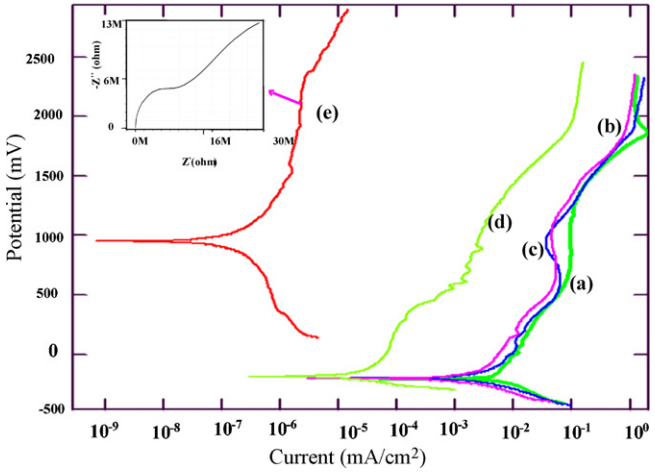

Fig. 7. Potentiodynamic polarization plots of (a) bare substrate, (b) AT plasma sprayed coating, (c) YSZ plasma sprayed coating, (d) bilayered plasma sprayed coating (BL-1) and (e) bilayered plasma sprayed coating (BL-2) (inset Nyquist plot of bilayered coating).

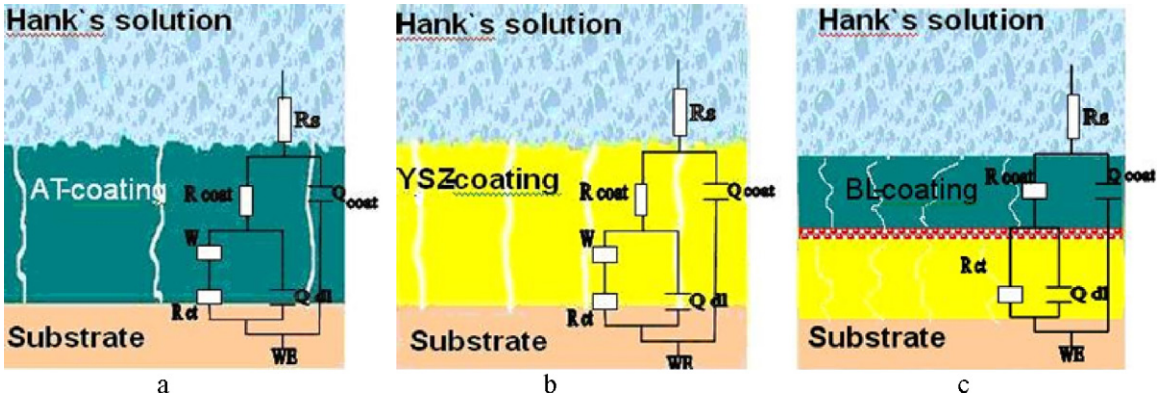

Fig. 8. Schematic diagrams representing the typical defects in the microstructure of plasma sprayed YSZ, AT and BL coatings responsible for the corrosion behaviour along with their equivalent circuits.

3.3. Potentiodynamic anodic polarization studies

Fig. 7 shows the potentiodynamic polarization plots obtained for the bare substrate and the plasma sprayed coatings in Hank's solution. There has been a significant shift in OCP towards the noble direction for the plasma sprayed BL coatings (Fig. 7e). This shift of OCP towards noble direction indicates the high passivating nature of the bilayered coating. The i_{corr} was the lowest for the BL coatings (BL-1 = 0.025 μA cm^{-2} and BL-2 = 0.07 nA cm^{-2}) when compared to that of the AT (1.2 μA cm^{-2}), YSZ (4.3 μA cm^{-2}) coatings and substrate (4.49 μA cm^{-2}). Similarly, the corrosion rates were 1.42×10^{-6} mm yr^{-1}, 0.0005 mm yr^{-1}, 0.023 mm yr^{-1}, 0.086 mm yr^{-1} and 0.089 mm yr^{-1}, respectively, for BL-2, BL-1, AT, YSZ and substrate, respectively. The higher corrosion resistance of BL coating is attributed to the presence of large amount of melted particles and lower porosity present in the BL coatings. The lower corrosion resistance of AT and YSZ coatings may be attributed to the presence of high porosity (0.6%) in AT and the presence of poorly consolidated splats and cracks in YSZ. The equivalent circuits used to fit the EIS parameters along with the schematic of the microstructures are shown in Fig. 8. We assume that a very thin dense interface layer would have formed in between these two layers which would have enhanced the corrosion resistance (Fig. 8c).

The Nyquist plot of bare substrate showed two time constants. The first time constant can be attributed to the resistance between the electrolyte and very thin oxide film present on the titanium alloy substrate and the second time constant may be attributed to the substrate alloy. The very low corrosion resistance offered by the substrate is due to the poor quality of the oxide film. The Nyquist plot of YSZ plasma sprayed coating shows two time constants and Warburg behaviour. The Warburg behaviour may be ascribed to the resistance offered due to the corrosion products blocking the pores/cracks present in the coating. AT plasma sprayed coating also showed Nyquist plot similar to that of YSZ coating. The Nyquist plot of BL-2 coating exhibited two time constants and no Warburg component was observed (Fig. 7 inset). The absence of Warburg component may be attributed to the presence of lower porosity in the BL coating.

4. Conclusions

Nanostructured YSZ and AT powders were plasma sprayed on biomedical Ti–13Nb–13Zr alloy. For the first time we report a plasma sprayed bilayer coating containing YSZ and AT layer. The BL coating possesses substantially a higher microhardness value (1096 ± 10 HV) which is ∼1.3 times that of AT (820 ± 22 HV) and ∼1.8 times that of YSZ coatings (617 ± 25 HV). The BL coating showed lower porosity compared to AT and YSZ coatings. The studies reveal high porosity and loosely bound unmelted alumina particles in the AT coating and the presence of poorly consolidated splat and cracks in the YSZ coatings. The average surface roughness of the coatings was in the range of 6–10 μm. The corrosion studies showed lowest i_{corr} for the BL coatings (BL-1 = 0.025 μA cm^{-2} and BL-2 = 0.07 nA cm^{-2}) when compared to that of the AT (1.2 μA cm^{-2}), YSZ (4.3 μA cm^{-2}) coatings and substrate (4.49 μA cm^{-2}). Thus BL plasma sprayed coatings of YSZ/AT seem to be a more promising route for improving the corrosion resistance of biomedical Ti–13Nb–13Zr alloy rather than the monolayer coatings of YSZ and AT. The scratch resistance and wear resistance properties of the coatings are in progress and will be communicated elsewhere.

Acknowledgments

The authors Sathish and Geetha thank the Department of Science and Technology for the funding. The authors thank Director of CSIR-NAL, Bangalore for the encouragement. The authors thank Mr. V.K. William Grips, Mr. Manikandanath, and Mr. Siju, NAL for the useful discussions on corrosion studies, Raman and FESEM studies, respectively. The authors also thank Dr. A.K. Singh and T.K. Nandy, DMRL, Hyderabad for providing Ti–13Nb–13Zr alloy substrates.

References

[1] M. Geetha, A.K. Singh, R. Asokamani, A.K. Gogia, Ti based biomaterials, the ultimate choice for orthopaedic implants—a review, Prog. Mater. Sci. 54 (2009) 397–425.

[2] F. Yildiz, A.F. Yetim, A. Alsaran, I. Efeoglu, Wear and corrosion behavior of various surface treated medical grade titanium alloy in bio-simulated environment, Wear 267 (2009) 695–701.

[3] L. Thair, U. Kamachi Mudali, N. Bhuvaneswaran, K.G.M. Nair, R. Asokamani, B. Raj, Nitrogen ion implantation and in vitro corrosion behavior of as-cast Ti–6Al–7Nb alloy, Corros. Sci. 44 (2002) 2439–2457.
[4] Y. Fu, X. Zhu, B. Tang, X. Hu, J. He, K. Xu, A.W. Batchelor, Development and characterization of CrN films by ion beam enhanced deposition for improved wear resistance, Wear 217 (1998) 159–166.
[5] M.F. Morks, N.F. Fahim, A. Kobayashi, Structure, mechanical performance and electrochemical characterization of plasma sprayed SiO_2/Ti-reinforced hydroxyapatite biomedical coatings, Appl. Surf. Sci. 255 (2008) 3426–3433.
[6] E.H. Jordan, M. Gell, Y.H. Sohn, D. Goberman, L. Shaw, S. Jiang, M. Wang, T.D. Xiao, Y. Wang, P. Strutt, Fabrication and evaluation of plasma sprayed nanostructured alumina–titania coatings with superior properties, Mater. Sci. Eng. A 301 (2001) 80–89.
[7] Y. Wang, S. Jiang, M. Wang, S. Wang, T. Danny Xiao, R. Peter Strutt, Abrasive wear characteristics of plasma sprayed nanostructured alumina/titania coatings, Wear 237 (2000) 176–185.
[8] L.T. Kabacoff, Nanoceramic coatings exhibit much higher toughness and wear resistance than conventional coatings, AMPITAC News Lett. 6 (1) (2002) 37–42.
[9] R.S. Lima, B.R. Marple, Thermal spray coatings engineered from nanostructured ceramic agglomerated powders for structural, thermal barrier and biomedical applications: a review, J. Therm. Spray Technol. 16 (2007) 40–63.
[10] S.F. Hulbert, Introduction to bioceramics, in: L.L. Hench, J. Wilson (Eds.), The Use of Alumina and Zirconia in Surgical Implants, World Scientific, Singapore, 1993, pp. 25–40.
[11] I.C. Clarke, H.A. McKellop, P. McGuire, R. Okuda, A. Sarmiento, Titanium alloys in surgical implants, in: H.A. Luckey, F. Kubli, Jr. (Eds.), Wear of Ti–6A1–4V Implant Alloy and Ultra-High Molecular Weight Polyethylene Combinations, American Society for Testing and Materials, ASTM STP 796, Philadelphia, 1983, pp. 173–186.
[12] J. Jerome Chevalier, S. Deville, E. Munch, R. Juillian, F. Lair, Critical effect of cubic phase on aging in 3 mol% yttria-stabilized zirconia ceramics for hip replacement prosthesis, Biomaterials 25 (2004) 5539–5545.
[13] W. Ma, H.Y. Dong, H. Guo, S. Gong, Thermal cycling behaviour of $La_2Ce_2O_7$/8YSZ double-ceramic-layer thermal barrier coatings prepared by atmospheric plasma spraying, Surf. Coat. Technol. 204 (2010) 3366–3370.
[14] S. Sathish, V. Anbarasan, M. Geetha, R. Asokamani, Corrosion resistance of laser nitrided commercially pure titanium and Ti–13Nb–13Zr biomedical alloys, Trans. Indian Inst. Met. 61 (2008) 235–238.
[15] A. Ghosh, A.K. Suri, M. Pandey, S. Thomas, T.R. Rama Mohan, B.T. Rao, Nanocrystalline zirconia–yttria system—a Raman study, Mater. Lett. 60 (2006) 1170–1173.
[16] E. Sanchez, E. Bannier, V. Cantavella, M.D. Salvador, E. Klyatskina, J. Morgiel, J. Grzonka, A.R. Boccaccini, Deposition of Al_2O_3–TiO_2 nanostructured powders by atmospheric plasma spraying, J. Therm. Spray Technol. 17 (2008) 329–337.
[17] X. Lin, Y. Zeng, X. Zhou, C. Ding, Microstructure of alumina–3 wt% titania coatings by plasma spraying with nanostructured powders, Mater. Sci. Eng. A 357 (2003) 228–234.
[18] R. Mcpherson, On the formation of thermally sprayed alumina coatings, J. Mater. Sci. 15 (1980) 3141–3149.
[19] L. Dubourg, R.S. Lima, C. Moreau, Properties of alumina–titania coatings prepared by laser-assisted air plasma spraying, Surf. Coat. Technol. 201 (2007) 6278–6284.
[20] N. Dejang, A. Watcharapasorn, S. Wirojupatump, P. Niranatlumpong, S. Jiansirisomboon, Fabrication and properties of plasma-sprayed Al_2O_3/$13TiO_2$ composite coatings: a role of nano-sized TiO_2 addition, Surf. Coat. Technol. 204 (2010) 1651–1657.
[21] D. Wang, Z. Tian, L. Shen, Z. Liu, Y. Huang, Microstructural characteristics and formation mechanism of Al_2O_3–13 wt% TiO_2 coatings plasma sprayed with nanostructure agglomerated powders, Surf. Coat. Technol. 203 (2009) 1298–1303.
[22] D. Wang, Z. Tian, L. Shen, Z. Liu, Y. Huang, Influences of laser remelting on microstructure of nanostructured Al_2O_3–13 wt.% TiO_2 coatings fabricated by plasma spraying, Appl. Surf. Sci. 255 (2009) 4606–4610.
[23] R. Tomaszek, Z. Pawlowski, J. Crimblot, J. Laureyns, Microstructural transformations of TiO_2, Al_2O_3 + $13TiO_2$ and Al_2O_3 + $13TiO_2$ at plasma spraying and laser engraving, Surf. Coat. Technol. 185 (2004) 137–149.
[24] E.P. Song, J. Ahn, S. Lee, N.J. Kim, Microstructure and wear resistance of nanostructured Al_2O_3–8 wt% TiO_2 coatings plasma-sprayed with nanopowders, Surf. Coat. Technol. 201 (2006) 1309–1315.
[25] O. Sarikaya, Effect of the substrate temperature on properties of plasma sprayed Al_2O_3 coatings, Mater. Des. 26 (2005) 53–57.
[26] H. Lu, X. Shi, M. Costa, C. Huang, Carcinogenic effect of nickel compounds, Mol. Cell Biochem. 279 (2005) 45–67.